ELSEVIER

Journal of Nuclear Materials 266–269 (1999) 67–74

journal of nuclear materials

Divertor erosion in DIII-D

D.G. Whyte [a,e,*], R. Bastasz [b], J.N. Brooks [c], W.R. Wampler [b], W.P. West [e], C.P.C. Wong [e], O.I. Buzhinskij [d], I.V. Opimach [d]

[a] *University of California, San Diego, CA 92093-0417, USA*
[b] *Sandia National Laboratories, Albuquerque, NM, USA*
[c] *Argonne National Laboratory, Argonne, IL, USA*
[d] *TRINITI Laboratory, Troitsk, Russia*
[e] *General Atomics, P.O. Box 85608, San Diego, CA 92186-5608, USA*

Abstract

Net erosion rates of carbon target plates have been measured in situ for the DIII-D lower divertor. For attached divertors ($T_e > 40$ eV), outer strike point (OSP) erosion rates exceed 10 cm/exposure-year, physical sputtering is dominant and the effective sputtering yield, Y, is greater than 10%. In detached divertors ($T_e < 2$ eV), the cold incident plasma eliminates physical sputtering and net erosion is suppressed at the OSP, which becomes a region of net redeposition (~4 cm/exposure-year). Molecular spectroscopy indicates an upper limit of $Y \leqslant 0.1\%$ for the chemical sputtering yield. The private flux wall is measured to be a region of net redeposition with dense, high neutral pressure, attached divertor plasmas. Leading edges intercepting parallel heat flux (~50 MW/m^2) have very high net erosion rates (~10 μm/s) at the OSP of an attached plasma.

Keywords: Carbon erosion; Chemical erosion; DiMES; Detached plasma; DIII-D

1. Introduction

Net erosion of plasma facing materials (PFM) is one of the most important problems to solve in designing power producing magnetic confinement fusion devices. The inherent poloidal asymmetry in plasma–material interactions (PMI) caused by the use of poloidal divertors concentrates particle flux, and therefore the regions of wall erosion outflux, onto a relatively small surface. High *net* erosion rates will lead to two or three operating limits in a steady-state device:

1. Plate lifetime, determined by the peak rate of net erosion.
2. Codeposited tritium inventory limits (for safety and fuel inventory) found in regions of net redeposition is determined by the poloidally integrated net erosion rate.
3. Core plasma impurity contamination, which limits power output due to fuel dilution and radiation losses, is also driven by the poloidally integrated erosion rate.

However, because the first two issues stated are of no concern in short pulse, present day machines, dedicated experiments to study and control net erosion have been less common than experiments dealing with wall 'conditioning' (e.g. reducing PFM gas recycling) and plasma impurity contamination.

Laboratory and tokamak erosion experiments have mostly focussed on obtaining physical and chemical sputtering yields for candidate materials, but these yields only address a portion of the net erosion problem, since it is strongly affected by the redeposition and transport of the materials. This redeposition is mostly determined by the incident plasma properties (e.g. mean free path of ionization). The net erosion is further complicated by the non-linearity caused by self-sputtering yields approaching unity. Finally, the 2-D transport of the impurities in the tokamak core/SOL plays a role in the poloidal 're-arrangement' of impurities, and hence in the

* Corresponding author. Tel.: +1 619 455 4127; fax: +1 619 455 2266; e-mail: whyte@gav.gat.com

0022-3115/99/$ – see front matter
PII: S0022-3115(98)00572-8

net erosion. These phenomena interact in a complex manner, making in situ measurements of net erosion necessary on current devices (e.g. DIII-D [1], JET [2], ASDEX-Upgrade [3]).

This paper will describe a campaign to measure the net erosion/redeposition rates in the divertor of the DIII-D tokamak under several operational conditions. The principal tool for this study is the Divertor Material Evaluation Studies (DiMES) sample probe [1]. Dedicated experiments are designed to carefully control and diagnose the sample exposure to allow comparisons between the sample's net erosion measurements, other erosion measurements (e.g. spectroscopy for gross erosion), the core plasma's impurity concentration and modeling of the erosion. It will be shown that:

1. Typical divertor net erosion rates of graphite in DIII-D during attached plasma operation would be unacceptable in a steady-state device, with peak net erosion rates greater than 10 cm/exposure-year – Note: defined as loss of target thickness that would occur during one year ($\sim 3 \times 10^7$ s) of plasma exposure;
2. 'Leading edges' of PFMs have very high net erosion rates and contribute significantly to hydrogenic codeposition;
3. Divertor 'detachment' reduces the heat flux a factor of 5–10 at the OSP compared to an attached divertor with the same input power and results in net redeposition of carbon in this region.

2. Net erosion measurements for graphite

The experimental method for measuring net erosion with DiMES has been previously described [4,5] and is briefly described here. A graphite sample is inserted whose surface is flush to the tiles of the DIII-D lower divertor, which are also graphite (Union-Carbide ATJ), making the sample a part of the floor. The divertor plasma geometry and outer strike-point (OSP) position is controlled during the discharge to expose the 50 mm diameter DiMES sample only to steady-state divertor plasma conditions (Fig. 1).

Samples are exposed to several discharges (typical total exposure is 10–20 s). Identical non-exposure discharges with slow radial sweeps of the OSP provide detailed radial profiles of divertor plasma parameters (electron density and temperature: n_e, T_e, ion flux: (Γ_i), tile temperature, incident heat flux: q). Pre- and post-exposure ion beam analysis (IBA) of the silicon (Si) depth marker implanted in the graphite samples determines net erosion/deposition to ± 10 nm [6].

2.1. Low power ELM-free and ELMing attached OSP

The OSP region net erosion has been studied in two cases of low recycling, low density divertor plasmas:

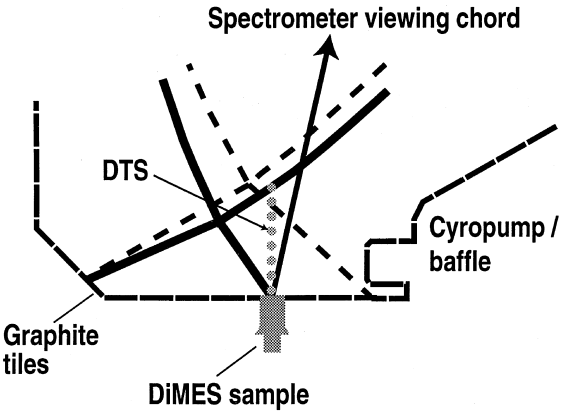

Fig. 1. Exposure geometry for DiMES experiments. Solid separatrix outline: OSP erosion experiments. Dashed separatrix outline: PF erosion experiments. Location of divertor spectrometer/D_α viewing chord and divertor Thomson scattering (DTS) is also shown.

Case (1) ELM-free H-mode, Case (2) ELMing H-mode. The plasma parameters for these discharges are: $P_{inj} \sim 2.5$–3 MW, $I_p \sim 1.4$ MA, $n_{e,OSP} \sim 1.2 \times 10^{19}$ m^{-3}, $T_{e,OSP} \sim 45$–70 eV, $\Gamma_i \sim 3 \times 10^{22}$ s^{-1} m^{-2}, $q \sim 0.7$ MW m, field line angle of incidence, $\theta \sim 2°$. As previously reported [4,7] the peak net erosion rate was $V_{net} = 3.6 \pm 0.7$ nm/s for Case 1, and $V_{net} = 3.0 \pm 0.7$ nm/s for Case 2. (Note: 1 nm/s $\sim$ 3 cm/exposure-year $\sim 1 \times 10^{20}$ atoms m^{-2} s^{-1} for carbon with atomic concentration, $n_c \sim 1 \times 10^{29}$ m^{-3}.) The quantity and features of net erosion have been modeled successfully using the WBC/REDEP [8,9] erosion simulation codes (Fig. 2). It is noted that in order to minimize effects from plasma startup/shutdown, the samples are kept in the private flux (PF) region ($\sim$1.5 s of ohmic plasma per exposure shot) until steady-state divertor conditions are reached. Based on measurements of samples exposed only to the PF region (Section 2.4) the expected net redeposition rate is <0.1 nm/s, which is within the uncertainty of the erosion rate measurement. ELMs deliver $\sim$20–25% of the incident heat flux in Case 2 [10], yet play a minor role in the net erosion under these conditions.

2.2. High power ELMing attached OSP

The OSP net erosion was measured in plasma discharges with more injected neutral beam power ($P_{inj} \sim 7$ MW) than described in Section 2.1. Other plasma parameters were similar: $I_p \sim 1.4$ MA, single lower divertor with no pumping, and an ELMing H-mode confinement regime (stored energy $\sim$ 1 MJ). This results in an attached plasma with OSP plasma parameters

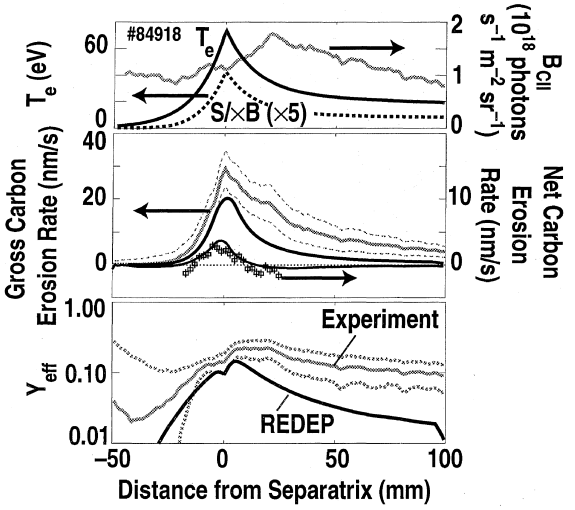

Fig. 2. Radial profiles near OSP in low power attached plasmas. (Top) Measured plasma temperature and CII brightness and calculated ionization/photon ratio (S/*XB*). (Middle) Measured (gray line and points) and REDEP predicted (dark line) gross (ELM-free case) and net (ELMy case) carbon erosion rates. (Bottom) Measured and REDEP predicted effective sputtering yield.

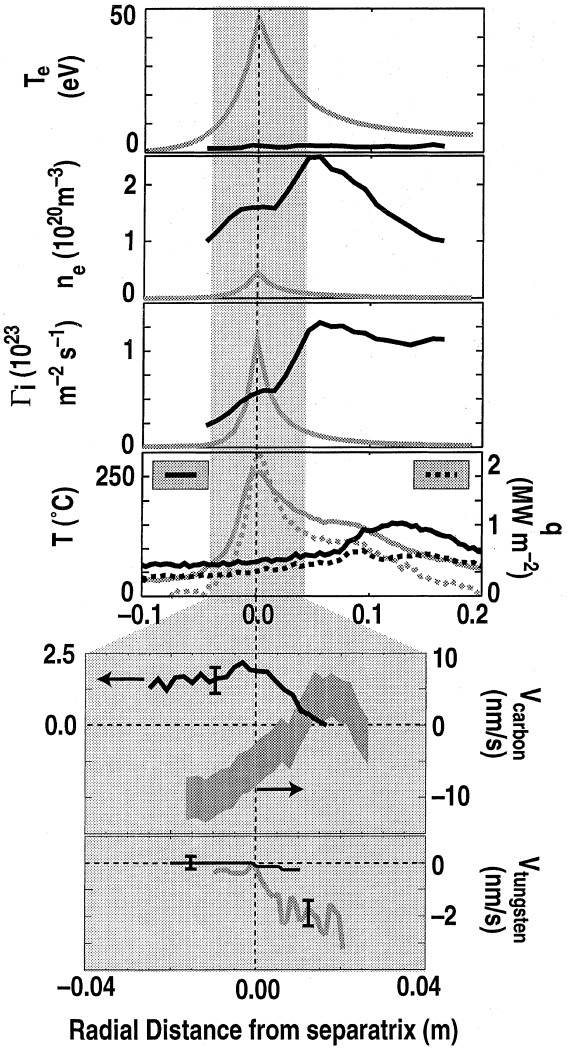

Fig. 3. OSP plasma parameters and carbon/tungsten erosion 'velocity' (rate of change of target thickness: $V_e < 0$ indicates erosion, $V_e > 0$ indicates net redeposition) versus radial distance from OSP. Light line: attached plasma (Section 2.2 Dark line: detached plasma (Section 2.3).

(Fig. 3) that have similar radial profiles and T_e to the low power cases, but with higher density, ion flux and power flux ($q \sim 2$ MW m^{-2})

The attached case shows a toroidal pattern of deposition/erosion similar to those previously reported [4] at these plasma conditions (i.e. attached, $q \sim 2$ MW/m^2). The cause of this pattern was speculated to be a toroidally localized, enhanced erosion source caused by a 0.1 mm height misalignment between the DiMES sample and the toroidally adjacent downstream tile (i.e. in the direction of the magnetic field). However, the misalignment was rectified for the current experiment. The DiMES sample was placed in a rooftop style alignment, with the toroidally adjacent tiles being ~0.2 mm higher upstream and 0.2 mm lower downstream, eliminating any 'leading edges'. Infrared thermography during exposure showed a very uniform (±10%) toroidal heating pattern across the sample and surrounding tiles. Visible light from a camera with a CII line filter directly viewing the sample indicated none of the previously observed 'hot spots' during quiescent periods (i.e. between ELMs). The persistence of the toroidal redeposition pattern (although the quantity of redeposition is reduced with the new alignment) suggests that the principal cause of the localized erosion source is ablation at the tile gaps (~3 mm) between the sample and surrounding tiles (Section 2.5 for details). Intermittent bright regions in both gap directions (i.e. radial and toroidal) were observed on several frames of the CII camera data, most likely caused by an ELM (and the associated high particle flux) during the measurement period (~16 ms). Nevertheless, the radial profile of the minimum erosion rate for the flat surface (Fig. 3) can be measured at the toroidal location on the sample where the least 'interference' from the localized source is expected. This toroidal position (about 10 mm upstream from the center) is the furthest away from the downstream tile, yet not in the region shadowed by the upstream tile (which is also a region of net redeposition [4,11]). This shows that the peak net erosion rate is $V_{net} \sim 10$–12 nm/s for the carbon just inboard of the OSP in the attached case.

2.3. Detached OSP

The use of divertor detachment in reducing the heat flux to the divertor plates is well established on DIII-D [12] and elsewhere [13]. A set of experiments was performed to assess the effect of divertor detachment on carbon net erosion rates at the OSP. The OSP net erosion was measured in plasma discharges with identical injected power ($P_{inj} \sim 7$ MW), plasma current ($I_p \sim 1.4$ MA), geometry (single lower divertor, no pumping) and confinement (ELMy H-mode, stored energy ~1 MJ) as those described in Section 2.2. In the detached case, a programmed D_2 gas injection (~100 Torr l/s) was used to increase the plasma density to $n_e \sim 1 \times 10^{20}$ m^{-3} from its initial normal value of $n_e \sim 4 \times 10^{19}$ m^{-3} in the attached case. The resulting differences in the OSP plasma parameters are shown in Fig. 3. The detached case shows the typical signatures of 'radiative divertor' experiments in DIII-D [14]: with $T_e \sim 1$–2 eV (measured with divertor Thomson scattering, DTS) over the entire OSP region, a radial 'spreading out' of the incident ion flux (with the peak ion flux appearing outboard from the OSP) and a 5–10 fold reduction in the heat flux at the OSP. The incident neutral flux (Γ_0) is an order of magnitude larger than the ion flux at $\sim 4 \times 10^{23}$ s^{-1} m^{-2} (as measured by a divertor pressure gauge, Section 3.3 assuming an incident energy of 2 eV for the neutrals (at these high densities $T_i \approx T_e \approx T_{neutral}$). The neutral flux can be assumed to be fairly spatially uniform due to the long mean free-path (MFP) of ionization for D neutrals.

In the detached case the *OSP carbon net erosion is eliminated and the OSP becomes a region of net redeposition*, with the build-up rate being ~1.5 nm/s (Fig. 3). As opposed to the attached case the redeposition exhibits toroidal uniformity on the sample. Surprisingly, there is weak experimental evidence of chemical erosion occurring at the OSP, as discussed in Section 3.2. Also included in Fig. 3 is the removal rate of a 100 nm tungsten (W) film (30 mm radial stripe, 3 mm toroidal extent, displaced 10 mm from sample's center) simultaneously exposed to the detached and attached OSP (see Ref.[4]). *The tungsten erosion rate is reduced in the detached case to a level smaller than the measuring sensitivity* (~0.2 nm/s).

2.4. Private flux region

Although plasma flux to the wall in the private flux (PF) wall region is weak compared to the strike-points, it represents a comparatively large surface area. Incident particle distribution is mostly dissociated hydrogenic neutrals (incident energy, $E_i \sim 1$–2 eV) and charge exchange neutral flux ($E_i > 5$ eV) from the X-point and divertor leg plasma [15]. Sputtered carbon from the PF has better geometric access to the X-point region, and therefore could play an important role in determining the carbon content of the core plasma [16].

A depth marked graphite DiMES sample was exposed for 28 s (~300 K surface temperature) in the PF region during a radiative divertor experiment on DIII-D. These lower single-null discharges ($P_{inj} \sim 8$ MW) have the OSP placed at the lower pump entrance ($R \sim 1.68$ m) and a large D_2 gas injection (>200 Torr l/s) at the midplane, in order to induce SOL flow. This is meant to enhance divertor compression of argon gas that is injected into the divertor through the PF region. This results in a highly radiative ($P_{div} \sim 5$ MW/m^3) and dense (outer divertor separatrix density $\sim 0.5 - 1 \times 10^{20}$ m^{-3}) attached outer divertor. The sample ($R = 1.48$ m) is 0.2 m from either strike-point and is located 0.2 m below the X-point (Fig. 1). A fixed position Langmuir probe provides the plasma parameters at the sample: $n_e \sim 2.0 \times 10^{18}$ m^{-3}, $T_e = 2 - 3$ eV, $\Gamma_i \sim 7 \times 10^{20}$ m^{-2} s^{-1}. The PF neutral pressure and fluxes will be discussed in Section 3.3.

IBA analysis of the Si depth marker indicates a radially *uniform net redeposition rate of* $\sim 7 \times 10^{19}$ m^{-2} s^{-1} (or $\sim 0.7 \pm 0.2$ nm/s $\sim 2.1 \pm 0.6$ cm/exposure-year) for the carbon. Therefore, the PF wall is a net *sink* for carbon under these conditions (which were chosen to maximize neutral flux and therefore erosion rates in the PF region, Section 3.3. If one expected only net erosion (i.e. no redeposition) caused by neutral chemical sputtering, the sensitivity of this experiment to chemical erosion yield is $Y < 2 \times 10^{-4}$.

2.5. Leading edges

The presence of leading edges (a PFM surface that intercepts parallel heat flux) is known to create impurity problems in tokamaks (e.g. re-designed tile geometry for JET [17]). A DiMES sample with a 0.7 mm vertical lip above the aligned surface (~ 30 mm radial extent) was exposed to the OSP of an ELMing H-mode plasma ($P_{inj} \sim 7$ MW, $T_{e,OSP} \sim 30$ eV, $n_e \sim 5 \times 10^{19}$ m^{-3}, $q \sim 2$ MW/m^2, $\theta \sim 2°$) for 0.5 s in order to study dust production caused by erosion [18]. Parallel heat flux ~50 MW/m^2 was incident on an area of 14 mm^2, which thermal analysis shows reached a temperature >2300°C. Redeposited carbon was collected on a recessed Si wafer (200 mm^2) facing the leading edge but receiving no direct plasma flux itself. IBA showed a uniform carbonaceous film of ~0.5 μm depth, while IR and Raman spectroscopy indicated a diamond-like structure and hardness for the film. From the ratios of the exposed and collection areas, the *net erosion rate of the leading edge is* $\geqslant 6$ μm/s (this neglects carbon deposition elsewhere on the sample). The deuterium/carbon ratio in the film is 12%, leading to *a hydrogenic codeposition* rate of 0.18 g s^{-1} m^2 *of exposed leading edge.*

3. Effective sputtering yields for graphite

3.1. Physical sputtering at attached OSP

An absolutely calibrated CCD camera, equipped with an interference filter, measures the radial profile of the brightness, $B(r)$, (photons s^{-1} m^{-2} sr^{-1}) of a C^{+1} (CII-5140 Å) spectral line for Case 1 in Section 2.1 (Fig. 2). Using the collisional-radiative (CR) excitation model from [19] and recommended ionization rates [20], the ionization/photon ratio (S/XB) is calculated for the experimental T_e and n_e profiles. Assuming that all C^{+1} ions are ionized in the field of view (poloidal ionization MFP <10 mm at OSP), then $4\pi B(r)$S/XB gives the gross carbon influx into the divertor plasma. Results show that near the OSP the measured carbon influx roughly matches REDEP modeling that includes oblique incidence and self-sputtering (Fig. 2). *The effective sputtering yield* (Y_{eff} = *gross carbon outflux/incident total ion flux*) *is* 10–20%, about four times larger than would be expected with normal incidence D, and no self-sputtering [7]. This result also shows that physical sputtering dominates over chemical sputtering ($T_{plate}\sim$ 100°C, $Y_{chem}\sim$ 1–2% [21]) for these high plasma temperature, low flux divertor regimes. The S/XB technique is questionable for $T_e < 10$ eV (i.e. 30–40 mm from OSP), because the ionization MFP for C^{+1} becomes too long (see relative error in Fig. 2).

The ratios of net to gross erosion for the sputtered carbon (Fig. 2) indicate a prompt redeposition efficiency $\geqslant$ 80–85% near the OSP in both the model and experiment (prompt signifies within a few ion gyroradii $\rho_i \leqslant 1$ mm $\sim \lambda_{MFP} \sim$ IBA spatial resolution). The fact that models and experiment show reasonable agreement for both the gross and net erosion gives greater confidence that the model is correctly treating the near surface transport and redeposition of the sputtered carbon.

3.2. Chemical sputtering at detached OSP

For the cold plasma temperatures and incident particle energies measured in detached plasmas (Section 2.3), chemical sputtering is the only expected source of erosion (i.e. $Y_{chem} \leqslant 10^{-2} \gg Y_{physical} \sim 0$) [21,22]. Therefore, it is useful to examine the expected and measured chemical erosion rates and their impact on the sample erosion.

The upper limits on the expected chemical sputtering yield of the target can be estimated from two methods: *Method* 1 Hydrocarbon molecular spectroscopy *and Method* 2 Comparisons of expected and measured redeposition. The results are summarized in Table 1.

Method 1: An absolutely calibrated visible spectrometer has several viewing chords that span the lower DIII-D divertor (Fig. 1). The CD radical (4308 Å, $A^2\Delta - X^2\Pi$) band was everywhere below the limit of detection ($B_{CD} \leqslant 1.5 \times 10^{16}$ photons s^{-1} m^{-2} sr^{-1}), including the viewing chord directly viewing the DiMES sample (Fig. 1) at the OSP. Monte-Carlo modeling of the OSP plasma erosion using WBC [23] predicts that ~50% of the hydrocarbon molecules (e.g. CD_4, C_2D_2, etc.) released from the OSP region will at some point dissociate through the CD radical state (others are redeposited as higher order molecules). Therefore, for this case the usual D/XB ~ 100 (dissociation/photon ratio for $T_e \leqslant 10$ eV) [24] is increased twofold and the spectroscopic upper limit on carbon out-flux from the plate is $\Gamma_{Carbon} \leqslant 4\pi B$D/XB $\sim 4.0 \times 10^{19}$ m^{-2} s^{-1}. Using the measured ion flux ($\Gamma_i = 3.0 \times 10^{22}$ s^{-1} m^{-2}) and neutral flux ($\Gamma_0 = 4.00 \times 10^{23}$ s^{-1} m^{-2}) at the OSP (Section 2.3), and two different assumptions about the relative yields of the neutrals to ions, gives the results listed in Table 1.

Method 2: The expected carbon deposition rate to the sample is estimated to be ~1.2–2.5 $\times 10^{20}$ s^{-1} m^{-2} or ~1.2–2.5 nm/s, from sources 'external' to the divertor. This is estimated from a simple calculation using the measured core/SOL carbon concentration [25] (f_c ~1.5%), the incident SOL plasma flux (~1.0 $\times 10^{23}$ s^{-1} m^{-2} at X-point from DTS) and divertor geometry. It is noted that the incident carbon from the core/SOL will mostly redeposit as neutrals (due to its recombination through the cold, $T \sim 1$ eV, plasma in front of the sample). The carbon recombination is confirmed by UEDGE modeling [26] and by the redeposition's toroidal uniformity (Section 2.4) extending into regions shadowed from ion flux. This implies that the local (i.e. divertor plate) *net* erosion contribution is <1 nm/s at the OSP. Including the preliminary result [23] that the prompt redeposition efficiency R is ~89% and the measured ion fluxes at the target gives an upper limit (i.e. $Y < \Gamma_{net,max}/\Gamma_{incident}/(1 - R)$) on the expected sputtering yield (Table 1). This method is highly sensitive to the calculated redeposition efficiency and the carbon

Table 1
Upper limit on total chemical sputtering yields in experiments for different assumptions about relative yields of ions and neutrals

Sputtering yield assumptions	Detached OSP: Method 1 CD spectroscopy	Detached OSP: Method 2 Expected redeposition	Private flux wall
Ions only, $Y_{neutral} = 0$	$<1.2 \times 10^{-3}$	$<3.6 \times 10^{-3}$	–
$Y_{ions} = Y_{neutral}$	$<8 \times 10^{-5}$	$<2 \times 10^{-4}$	$<2 - 3 \times 10^{-4}$

concentration at the X-point, quantities that cannot be measured directly. Therefore, the spectroscopic results (*Method* 1) are the more certain of the two methods, since they do not rely on assumptions about redeposition sources or efficiency. Nevertheless, the two methods give similar limits. Detailed modeling of the redeposition in the detached regime is underway.

From [21], the expected sputtering yield (at $E_i = 10$ eV, $T_{surface} \sim 350$ K, $\Gamma_{D+} = 3 \times 10^{18}$ m^{-2} s^{-1}) for methane is $Y(CD_4/D^+) \sim 4.5 \times 10^{-3}$, and the total hydrocarbon yield is $Y(C/D^+) \sim 10^{-2}$. If the flux dependence of $\Gamma^{-0.1}$ from [21] is taken into account, *the total yield would be expected to decrease to* $Y(C/D^+) \sim 5 \times 10^{-3}$, *approximately five times larger than the most reliable estimate of the* Y_{chem} limit from CD *spectroscopy*. It is noted that in our experiment incident ion energies ($E_i \sim 5\ T_e \sim 5$ eV) are below the lowest energy measured using ion beam techniques.

3.3. Chemical sputtering at private flux wall

The PF region is characterized by large neutral densities and fluxes as measured by two diagnostic methods for the exposure described in Section 2.4. The first uses a manometer pressure gauge that samples the neutral influx into a vertical port situated at the DiMES radial location (at another toroidal location). By using the DEGAS simulation result [15,27] that the majority of PF pressure is due to dissociated deuterium atoms ($E \sim 2$ eV, from Franck–Condon dissociation of D_2), their flux to the floor can be derived from the average measured pressure ($P \sim 15$ mTorr for these experiments), to give $\Gamma_0 \propto PE^{-1/2} \sim 1.0 \pm 0.3 \times 10^{23}$ m^{-2} s^{-1}. The neutral flux emanating from the PF region is also proportional to the D_α brightness measured at the outer divertor leg (Fig. 1). The measured D_α brightness ($\sim 3 \times 10^{20}$ photons s^{-1} m^2 sr^{-1}) is converted to incident flux using an ionization/photon (S/XB) ratio of 40 ± 10 giving $\Gamma_0 = 4\pi B$ S/XB $\sim 1.5 \pm 0.4 \times 10^{23}$ m^{-2} s^{-1}. The S/XB ratio is calculated using a CR atomic model [28] for the excitation and ionization rates and simulating the emissions from 2 eV incident deuterium neutrals along the line of sight using the plasma density and temperature profiles. The two techniques agree within uncertainties and both track each other linearly when the D_2 gas injection is increased. Therefore, the incident neutral flux to the sample is $\sim$200 times larger than the ion flux of $\Gamma_i \sim 7 \times 10^{20}$ m^{-2} s^{-1}, implying that neutrals will dominate chemical erosion processes.

As at the detached OSP, the CD molecular band brightness is below detection limit ($B_{CD} < 1.5 \times 10^{16}$ photons s^{-1} m^{-2} sr^{-1}) for the spectrometer viewing chord looking at DiMES and intercepting the outer divertor leg (Fig. 1). This molecular band has a roughly constant dissociation/photon ratio D/XB$\sim$100 [24] for $T_e < 30$ eV. This implies that the chemical erosion flux leaving the PF must be $\leqslant 2 \times 10^{19}$ m^{-2} s^{-1} and that the effective chemical sputtering yield is $Y(C/D) \leqslant 1 - 2 \times 10^{-4}$ for the incident neutrals at the PF wall. These upper limits are similar to values for thermally dissociated atomic hydrogen's chemical sputtering on pyrolitic graphite [29] ($Y \sim 0.5 - 2 \times 10^{-4}$ at 300 K). It is interesting to note that the simultaneous bombardment of ions ($\Gamma_i/\Gamma_0 \sim 10^{-2}$, with $E_i \sim 10{-}15$ eV) and higher energy charge-exchange neutrals in this experiment does not seem to lead to the large enhancement in Y_{chem} as reported in Ref. [29] (100 fold increase with $\Gamma_{Ar+}/\Gamma_H \sim 10^{-3}$).

There are two possible sources for the redepositing carbon flux at the PF wall. A carbon fraction of 10% in the incident plasma would result in $\sim 7.0 \times 10^{19}$ m^{-2} s^{-1} carbon ion influx to the plate. This fraction seems reasonable since previous studies of attached divertor plasmas on DIII-D have shown $f_{Cdivertor} > 10\%$ [19] and effective physical sputtering yields at the OSP are >10% (Section 3.1). The other possible source is redeposition of hydrocarbons resulting from higher chemical erosion out-flux near the strike-points (redeposition of chemically eroded hydrocarbons from the PF wall only reduces the net erosion, but cannot cause net redeposition). However, this source would result in a molecular flux into the divertor leg/X-point plasma and subsequent CD band emissions. Therefore, this source of redeposition is less likely but possible, since the flux limit of detection from CD band spectroscopy ($\sim 2 \times 10^{19}$ m^{-2} s^{-1}) is just less than the net redeposition rate (7×10^{19} m^{-2} s^{-1}).

4. Discussion

4.1. Implications of attached OSP erosion rates

A summary of the DIII-D OSP carbon erosion [1,4,30] is shown in Fig. 4. Included for comparison is the measured CFC target's OSP erosion rate for a JET hot ion H-mode [2]. Apparently, carbon's net erosion rate consistently increases with the incident heat flux for attached plasma conditions. Note that even at modest q (<1 MW/m^2) the attached OSP has a net erosion rate that would seem unacceptable for a steady-state device (>10 cm/exposure-year) since the typical plate thickness is limited $\sim$1–3 cm for heat conduction purposes. Because of the large effect of ionization MFP on net erosion, scaling of the erosion rate with n_e at constant q is an important task for the future.

4.2. Implications of reduced erosion in detached plasma

The suppression of net erosion at the OSP during divertor detachment is encouraging because it eliminates the very large localized erosion source seen there during

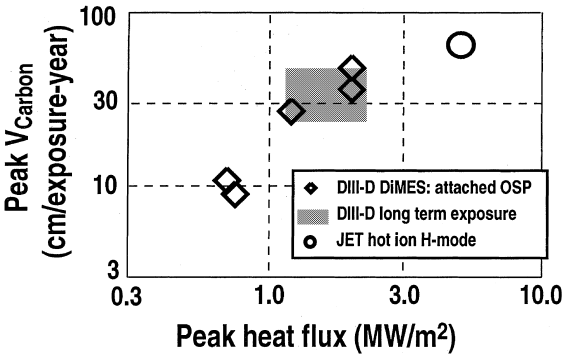

Fig. 4. Summary of peak net carbon erosion rates (cm/exposure-year) vs. peak incident heat flux for attached OSP plasmas (logarithmic plot). The erosion rates from a long-term (9 month, 1400 shots) exposure of lower divertor tiles [1] have been included. JET OSP erosion results from [2].

attached operations. However it should be noted that in the detached divertor, the peak in the ion flux is actually outboard of the OSP, and may be the region of net erosion at the outer divertor (as suggested by the trend of lower redeposition at the outboard side in Fig. 3). Future experiments will address this issue. It is also important to note that despite the differences in OSP erosion, *the detached and attached plasmas described in Sections* 2.2 *and* 2.3 *have the same core carbon density* (but f_C is lower in the detached case due to the higher n_e). This suggests that either the OSP is not a significant contributor to the core carbon in the attached phase or that the carbon source has 'shifted' to another poloidal location due to the detachment. Obviously, the presence of net redeposition at the OSP implies net erosion at another poloidal location(s). The determination of these locations, and their relative contribution to core contamination and plate erosion, is critical for evaluating the overall effectiveness of a given operational scenario.

The consistently low chemical sputtering yields inferred from the DIII-D experiments (detached OSP and PF) could be due to a combination of factors. The relatively cold plate temperatures ($\leqslant 350$ K), the efficient redeposition of hydrocarbons (due to the sonic plasma flow directed to the plate in detached plasmas) [31], the high flux ($Y \propto \Gamma^{-0.1}$) and the frequent boronizations of DIII-D all tend toward lowering chemical erosion. Whatever the cause, *the measured effective sputtering yield of carbon at the OSP is reduced about two orders of magnitude from* $Y_{eff} = 1-2 \times 10^{-1}$ *in the attached case to* $Y_{eff} \leqslant 10^{-3}$ for the detached case.

4.3. Implications of leading edge erosion

A concern caused by leading edges is the high codeposition on adjacent surfaces, as illustrated by an estimate from DIII-D. The 5 mm gaps between the divertor tiles of DIII-D behave similarly to the leading edge described in the DiMES exposure (Section 2.5). With perfectly horizontal tile alignment, each gap presents a leading edge $\sim$0.15 mm in height ($\theta \sim 2°$), but in practice the alignment tolerance is $\sim$0.4 mm. The side of the adjacent tile directly faces the leading edge and will collect redeposited carbon (and codeposition) in a manner similar to the silicon wafer. Taking an average strike-point (inner and outer) width of 40 mm, and with $\sim$80 toroidal tiles, gives the area of leading edge in the DIII-D lower divertor to be $\sim 0.5 - 1.0 \times 10^{-3}$ m^2. Previous analysis of DIII-D lower divertor tiles (exposed to 2000 shots or $\sim$5000 s) [32] showed that roughly half (0.5 g) of the total 1 g of codeposited deuterium in the lower divertor was found in the tile gaps. Using the DiMES measured codeposition rate (0.18 g s^{-1} per m^2) and DIII-D leading edges area predicts a codeposition rate of $\sim$0.5–1 g. Therefore, the high erosion rate caused by leading edges is a plausible explanation for the high percentage of carbon and hydrogenic redeposits found in tile gaps. This is a concern for large-scale D–T devices like ITER (with a divertor surface $\sim$100 m^2, with >10000 CFC tiles), not only because of the limited access into the gaps, but also because of the possibly erosion resistant diamond-like nature of the redeposits [18].

Rooftop alignment of tiles eliminates leading edges but leads to areas of large redeposition in shadowed areas [11], and decreases the effective divertor area for heat removal. Operational experience in DIII-D has found that placing the OSP in new poloidal locations, or reversing the magnetic orientation (and hence finding 'new' leading edges), leads to enhanced carbon impurities until sufficient 'conditioning' of these edges occurs over several shots. This is consistent with the observation that the typical leading edge is $\geqslant$ 0.1 mm, and would erode at a rate $\sim$0.01 mm/s (Section 2.5) therefore taking tens of seconds (or several shots) to rectify. Note that leading edges are also a concern for *toroidal* gaps (i.e. between adjacent radial tiles), since the field lines have a finite radial component ($B_r/B \sim 0.02$ at OSP) that would create leading edges there as well as at the radial gaps.

5. Conclusion

Net erosion rates of carbon have been measured in the DIII-D divertor. The erosion rates at an attached outer strike-point (OSP) are >10 cm/exposure-year, even with incident heat flux <1 MW/m^2. OSP erosion is dominated by physical sputtering and effective yields are greater than 10%. At 2 MW/m^2, attached OSP erosion rates are $\sim$50 cm/exposure-year. Divertor plasma detachment decreases the incident plasma temperature below 2 eV. Tungsten erosion is eliminated during

detached operations, indicating the absence of physical sputtering. The absence of measurable hydrocarbon molecular band radiation places an upper limit on the *chemical* sputtering yield ~0.1%. This low chemical erosion yield, and the elimination of physical sputtering, suppresses net carbon erosion at the outer strike-point. The private flux wall is a region of net redeposition with dense, high neutral pressure attached plasmas. Leading edges have net erosion ~10 μm/s at the OSP of an attached plasma. The erosion of leading edges caused by tile gaps can account for half of the codeposition in the DIII-D divertor.

Acknowledgements

We acknowledge the technical support of T. Carlsness. This work was supported by the US Department of Energy under contracts DE-AC04-94AL85000 (Sandia), W-31-109-Eng-38 (Argonne) and DE-AC03-98ER54411 (General Atomics).

References

[1] C.P.C. Wong, R. Junge, R.D. Phelps et al., J. Nucl. Mater. 196–198 (1992) 871.
[2] H.Y. Guo, J.P. Coad, S.J. Davies et al., J. Nucl. Mater. 241–243 (1997) 385.
[3] K. Krieger, J. Roth, A. Annen et al., J. Nucl. Mater. 241–243 (1997) 684.
[4] D.G. Whyte, J.N. Brooks, C.P.C. Wong et al., J. Nucl. Mater. 241–243 (1997) 660.
[5] R. Bastasz, W.R. Wampler, J.W. Cuthbertson et al., J. Nucl. Mater. 220–222 (1995) 310.
[6] W.R. Wampler, R. Bastasz, D. Buchenauer et al., J. Nucl. Mater. 233 (1995) 791.
[7] J.N. Brooks, D.G. Whyte, Nucl. Fusion (submitted).
[8] J.N. Brooks, Nucl. Technol./Fusion 4 (1983) 33.
[9] N.J. Brooks, Physics Fluids B (Plasma Phys.) 2 (1990) 1858.
[10] A.W. Leonard, W. Suttrop, T.H. Osborne et al., J. Nucl. Mater. 241–243 (1997) 628.
[11] J.P. Coad, M. Rubel, C.H. Wu, J. Nucl. Mater. 241–243 (1997) 408.
[12] T.W. Petrie, D.N. Hill, S.L. Allen et al., Nucl. Fusion 37 (1997) 321.
[13] G.F. Matthews, J. Nucl. Mater. 220–222 (1995) 104.
[14] M.E. Fenstermacher, R.D. Wood, S.L. Allen et al., J. Nucl. Mater. 241–243 (1997) 666.
[15] M.E. Fenstermacher, G.D. Porter, M.E. Rensink et al., J. Nucl. Mater. 220–222 (1995) 330.
[16] K. Shimizu, T. Takizuka, A. Sakasai, J. Nucl. Mater. 241–243 (1997) 167.
[17] D.J. Campbell, J. Nucl. Mater. 241–243 (1997) 379.
[18] O.I. Buzhinskij, I.V. Opimach, V.A. Barsuk et al., these Proceedings.
[19] R.C. Isler, R.D. Wood, C.C. Klepper et al., Phys. Plasma 4 (1997) 355.
[20] M.A. Lennon, K.L. Bell, H.B. Gilbody et al., J. Phys. Chem. Ref. Data 17 (1988) 1285.
[21] J.W. Davis, A.A. Haasz, J. Nucl. Mater. 241–243 (1997) 37.
[22] W. Eckstein, C. Garcia-Rosales, J. Roth et al., Sputtering Data, IPP, Garching, Germany, IPP 9/82, 1993.
[23] J.N. Brooks, D. Alman, F. Federici et al., these Proceedings.
[24] Y. Ra, A. Pospieszczyk, Y. Hirooka et al., J. Vacuum Sci. Technol. A (Vacuum, Surfaces, and Films) 8 (1990) 1783.
[25] D.G. Whyte, M.R. Wade, D.F. Finkenthal, K.H. Burrell, P. Monier-Garbet, B.W. Rice, D.P. Schissel, W.P. West, R.D. Wood, Nucl. Fusion 38 (1998) 387.
[26] G.D. Porter, personal communication, DIII-D, San Diego, USA, 1997.
[27] M.E. Fenstermacher, personal communication, DIII-D, San Diego, USA, 1998.
[28] H.P. Summers, Atomic Data and Analysis Structure – User Manual, JET Joint Undertaking, Abingdon, UK, JET-IR(94), 1994.
[29] E. Vietzke, K. Flaskamp, V. Philipps, J. Nucl. Mater. 111–112 (1982) 763.
[30] F. Weschenfelder, G.L. Jackson, P. Wienhold et al., Plasma Phys. Controlled Fusion 38 (1996) 1043.
[31] A.W. Leonard, M.A. Mahdavi, S.L. Allen et al., Phys. Rev. Lett. 78 (1997) 4769.
[32] D.S. Walsh, B.L. Doyle, G.L. Jackson, J. Vacuum Sci. Technol. A (Vacuum, Surfaces, and Films) 10 (1992) 1174.